Cement and Concrete Research 48 (2013) 25–33

Contents lists available at SciVerse ScienceDirect

Cement and Concrete Research

journal homepage: http://ees.elsevier.com/CEMCON/default.asp

Application of wire beam electrode technique to investigate initiation and propagation of rebar corrosion

Wei Shi, Ze Hua Dong *, De Jie Kong, Xing Peng Guo

School of Chemistry and chemical engineering, Huazhong University of Science and Technology, Wuhan, 430074, China

ARTICLE INFO

Article history:
Received 31 March 2012
Accepted 18 February 2013

Keywords:
Reinforcement (D)
Corrosion (C)
Acceleration (A)
Electrochemical properties (C)
Mortar (E)

ABSTRACT

Multi-electrode technique named as wire beam electrode (WBE) was used to study pitting corrosion of rebar under concrete cover. When WBE embedded mortar sample was immersed in NaCl solution, uneven distributions of galvanic current and open circuit potential (OCP) on the WBE were observed due to the initiation of pitting corrosion. The following oxygen depletion in mortar facilitated the negative shift of the OCP and the smoothing of the current and potential distributions. Wetting–drying cycle experiments showed that corrosion products instead of oxygen in wet mortar specimen sustained the propagation of pitting corrosion due to Fe (III) taking part in cathodic depolarization during oxygen-deficient wet period, which was confirmed by micro-Raman spectroscopy. In addition, new pitting corrosion occurred mainly near the corrosion products, leading to preferentially horizontal propagation of rust layer on the WBE. A localized corrosion factor was further presented to quantify the localised corrosion based on galvanic current maps.

1. Introduction

Carbon steel rebar embedded in concrete is passive by forming a thin layer of hydroxides due to the concrete alkalinity [1,2]. Considering marine exposure conditions and extensive use of de-icing salts in many countries, chloride induced corrosion is one of the most common causes of degradation of reinforced concrete structures [3,4]. In the presence of aggressive ions (mainly chlorides), the passive film on steel is damaged and the corrosion rate become significant [5]. On the other hand, CO_2 reacts with the alkaline compounds in the pore solution of concrete leading to pH decrease and consequent loss of passivation of the rebar [6,7].

The corrosion of carbon steel in concrete is highly heterogeneous in the initial period of corrosion. As one of the most common corrosion, pitting corrosion (a type of localized corrosion) is prone to take place in the area with sufficient chloride ions and low pH or physical heterogeneities such as inclusions, lattice or mill-scale defects and grain boundaries [8]. In addition, the concrete compactness and some environmental factors (natural environment such as oxygen content, humidity, temperature, acid rain or even microorganisms, etc.) can influence the initiation of pitting corrosion. Once a pit initiates, it may propagate rapidly [9].

Electrochemical methods such as half-cell potential, linear polarization resistance (LPR) and electrochemical impedance spectroscopy (EIS) were introduced for corrosion monitoring of rebar underneath concrete cover. However, these conventional methods could only provide general information of rebar corrosion rather than the initiation and propagation information of the localized corrosion on the rebar surface. A multi-electrode technique (also called wire beam electrode, WBE) composed of a large number of wire electrodes arranged together compactly was successfully applied in studies of heterogeneous corrosion [10]. WBE can simulate the electrochemical processes on a one-piece electrode by continuously mapping the potential and galvanic current on the surface of WBE [11], it can provide clear potential and current distributions, indicating the local cathodic and anodic areas on WBE under concrete cover.

Corrosion products of steel in concrete is a complex mixture of goethite (α-FeOOH), magnetite (Fe_3O_4), wustite (FeO), maghemite (γ-Fe_2O_3) and/or oxyhydroxide (lepidocrocite, γ-FeOOH) [12,13]. The balance between iron oxides mainly depends on the accommodation of local oxygen content, Cl^- and moisture [13,14]. Wang et al. found that the β-FeOOH in corrosion products could be reduced into FeO by consuming electrons from the anodic dissolution of carbon steel [15]. Wong et al. [16] found that corrosion products could accumulate at the steel/concrete interface as well as penetrate cement paste. Depending on levels of oxidation, corrosion products have specific volumes ranging from about two to six times that of the iron consumed [17]. Due to the expansive stress of rust layer, long and wide cracks can be formed in concrete, facilitating the ingression of Cl^- and CO_2 and accelerating the corrosion of rebar. Particularly, dense rust layer on rebars could hinder corrosion inhibitors to migrate and adsorb on the surface of rebars, leading to a significantly decrease of inhibitive efficiency [18].

However, there are few studies on the propagation of corrosion products and the diffusion of corrosion inhibitors along the interface

* Corresponding author. Tel.: +86 27 87543432.
E-mail address: zehua.dong@gmail.com (Z.H. Dong).

0008-8846/$ – see front matter © 2013 Elsevier Ltd. All rights reserved.
http://dx.doi.org/10.1016/j.cemconres.2013.02.009

of rebar/mortar. Therefore, this work aims at *in-situ* tracking the initiation of pitting corrosion and the propagation of corrosion products based on the potential and current distributions on WBE. In addition, the compositions of corrosion products were confirmed by micro-Raman spectroscopy [19–21].

2. Experimental

2.1. Material and methods

A WBE was fabricated of 100 identical wires (1.4 mm diameter) of Q345B mild steel with a total working area of 1.54 cm^2, all wires were arranged regularly as 5 × 20 rectangle array and embedded in epoxy resin with an interval of 0.3 mm from one another for electric insulation (Fig. 1) [22,23]. The rectangle WBE was adopted for studying the lengthwise diffusion process of chloride ions. The chemical composition of Q345B steel (wt.%) is: C 0.18, Mn 0.42, Si 0.30, P ≤ 0.035 and S ≤ 0.035, Fe balance. The exposed face of WBE was polished subsequently with 400, 800 and 1000 grit SiC paper and cleaned with deionised water and ethanol.

Fig. 2 shows schematically the electric circuits for the measurement of potential and galvanic current distributions on WBE via a multichannel zero resistance ammeter (ZRA) (CST520, Corrtest). The potential distribution of WBE is mapped by measuring sequentially the open circuit potential (OCP) of a chosen wire electrode (W_j) against a saturated calomel electrode (SCE) as reference, with W_j temporarily disconnected from the WBE. The current distribution is mapped by measuring the galvanic current between W_j and all other interconnected wire electrodes, with W_j and all other interconnected wire electrodes being connected to the positive and negative poles of the ZRA, respectively. During non-test period, all wire electrodes in the WBE were interconnected together so electrons could move freely between wires to simulate electrochemically a conventional one-piece electrode.

The mortar specimens were cast with ordinary Portland cement/standard sand (ISO679 EN 196-1)/water at a mass proportion of 1/2.5/0.5 [24]. Fresh mortar was compacted by a lab vibrator, with the WBE being mounted at the centre of a 60 × 40 × 40 mm rectangular mortar specimen, as shown in Fig. 3. After 24 h setting time, the mortar specimen were de-moulded and cured in water for 28 days. The WBE embedded mortar specimen was then inserted in the middle of a 150 × 40 × 40 mm glass fibre reinforced epoxy resin container, and the gap between the lateral sides of mortar specimen and the container was sealed by epoxy resin paste to ensure that Cl^- ions in the left bath only diffuse through the mortar specimen to the right bath without any leakage through gaps. Prior to measure the potential and current maps of WBE, both baths of the container

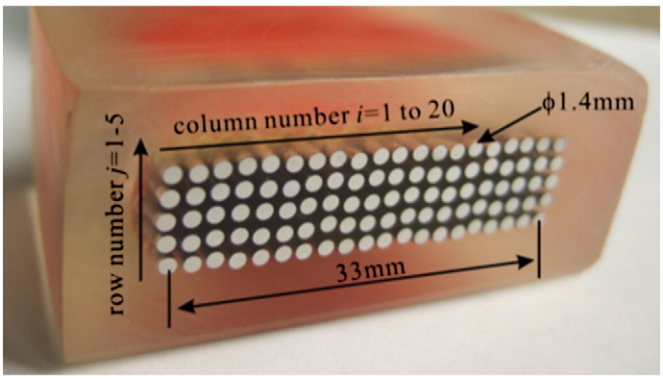

Fig. 1. 5 × 20 rectangular shape wire beam electrode (WBE).

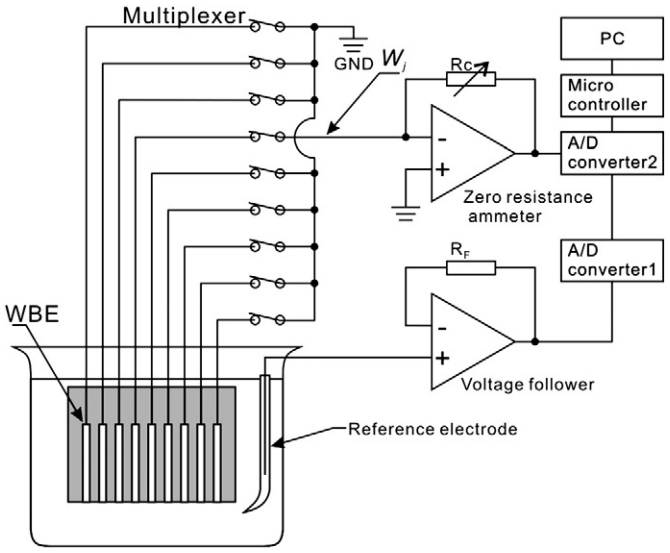

Fig. 2. Schematic circuits of a multichannel zero resistance ammeter (ZRA) applied to map the potential and current distributions of WBE embedding in mortar.

(Fig. 3) have been full of saturated $Ca(OH)_2$ solution for 3 days to ensure that the mortar was fully saturated with $Ca(OH)_2$.

Two routines were employed to accelerate corrosion of the WBE. The one was conducted with the left bath filled with 3% NaCl solution and the right bath with saturated $Ca(OH)_2$ solution during whole test. Another routine was carried out under wetting–drying cycle with drying to wetting period at 24 h: 24 h at 50 °C in a test chamber. During drying period, the mortar specimen was put into the chamber after solutions in the two baths drained off. During wetting period, the left and right baths were refilled with 3% NaCl and saturated $Ca(OH)_2$ solutions respectively, and 2 h later the potential and current distributions of WBE were mapped by ZRA.

After electrochemical tests were completed, the WBE-embedded mortar specimens were broken apart to expose corrosion products, and then the WBE samples were immediately transferred into a nitrogen-filled container to prevent oxidation of corrosion products. The corrosion products were analyzed by a DXR laser Raman microscope (Thermo scientific, USA) in 24 h. The spectra were excited with 532 nm radiation from a 35 mW air-cooled He-Ne laser and the laser beam was focused on the sample by an × 80 lens to give a spot size of *ca.*1 μm. The laser power was always kept below 0.7 mW to avoid sample degradation.

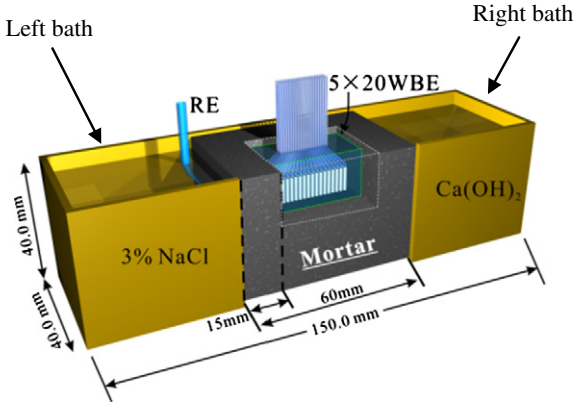

Fig. 3. Configuration of electrolytic container and installation of WBE-embedded mortar sample with the working surface of WBE facedown, RE represents saturated calomel electrode (SCE).

2.2. Analysis on the galvanic current of WBE

Galvanic current between wire electrodes is indicative of localized corrosion [25]. According to Evan diagram [8], Fig. 4 shows schematically the galvanic current between the jth (j = 0–99) wire electrode (W_j) in the WBE and the rest wire electrodes (W_R) interconnected through the ZRA, and the dependence of the general potential E_g of WBE on the OCP of the jth electrode W_j ($E_{j,corr}$). The anodic and cathodic current of each wire electrode can be expressed as Eq. (1).

$$I_{j,a} = I_{j,corr}\exp\left(\frac{E_{g,j}-E_{j,corr}}{\beta_{j,a}}\right),\ I_{j,c} = I_{j,corr}\exp\left(-\frac{E_{g,j}-E_{j,corr}}{\beta_{j,c}}\right) \quad (1)$$

where $I_{j,a}$, $I_{j,c}$ are the anodic and cathodic currents from W_j, $\beta_{j,a}$, $\beta_{j,c}$ the Tafel slopes of anodic and cathodic reactions on W_j, $I_{j,corr}$, $E_{j,corr}$ are the corrosion current and corrosion potential of W_j, respectively. E_g represents the general potential of the WBE with all wires interconnected together. The measured galvanic current $I_{g,j}$ is the difference of the $I_{j,a}$ and $I_{j,c}$, i.e. $I_{g,j} = I_{j,a} - I_{j,c}$. In addition, the mortar resistance forms an Ohmic (IR) drop between the potentials of W_j and W_R, i.e. $E_{g,R} - E_{g,j} = I_{g,j} \times R$.

According to Eq. (1), the galvanic current $I_{g,j}$ is actually equal to the polarization current just like that potential $E_{g,j}$ was applied on the wire electrode W_j. The direction of potential difference between the wire electrode W_j and the rest wire electrodes of WBE determines the galvanic polarity of W_j (anode or cathode) [26].

2.3. Quantification of Localized corrosion

WBE technique has been applied to study heterogeneous corrosion beneath coating [27], biofilms [10,28], soils [29], etc. However, most researches merely provided qualitative descriptions on the localized corrosion but failed to give a quantitative estimate on it. To describe the degree of localised corrosion based on the current statistics of wire electrodes, we prefer a so called "localized corrosion factor (LF)", as shown in Eq. (2).

$$LF = \sqrt{\sum_{j=1}^{N_a}\left(I_{j,g}^{a}\right)^2 \Big/ \sum_{i=1}^{100-N_a}\left(I_{i,g}^{c}\right)^2} \times \frac{N_c}{N_a} \quad (2)$$

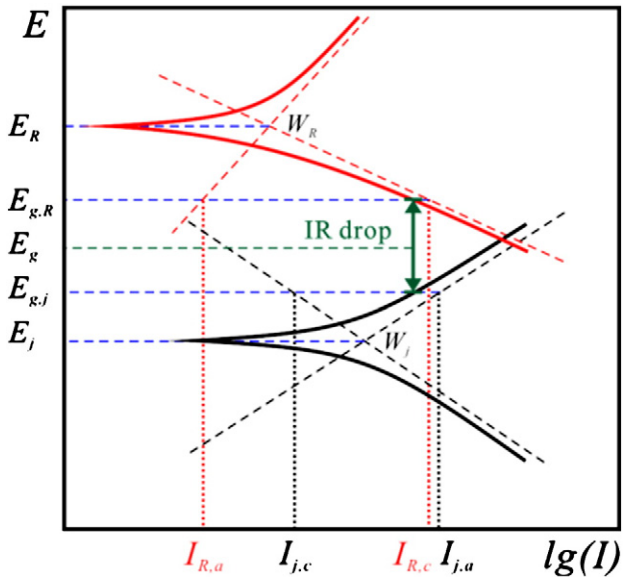

Fig. 4. Schematic formation of galvanic current between wire electrodes in WBE by Evans diagram. W_j, W_R represent the jth wire and the rest wires in WBE, E_g, $E_{g,R}$ and $E_{g,j}$ are the coupled potential of the whole WBE, W_R and W_j, respectively. E_R and E_j are the OCPs of the W_R and W_j, $I_{j,a}$, $I_{j,c}$, $I_{R,a}$ and $I_{R,c}$ are the anodic and cathodic current of W_j and W_R, respectively.

Where N_a, N_c are the total number of wire electrodes with anodic and cathodic current values, respectively. The sum of N_a and N_c is apparently the total number of wire electrodes in the WBE. $I_{j,g}^{a}$, $I_{i,g}^{c}$ are the galvanic values corresponding to the jth anodic and the ith cathodic wire electrodes, respectively. As mentioned before, the sum of anodic currents is equal to that of cathodic currents in the WBE, but the anodic regions may occupy less area compared to the cathodic regions when localized corrosion occurs. Thus the higher anodic density and lower cathodic density lead to a higher LF value, and the LF index would be therefore a good indication to the degree of localized corrosion.

2.4. EIS measurement for WBE

Electrochemical impedance spectrum (EIS) measurement was conducted to obtain exact corrosion information of each single wire in the WBE. EIS were measured by CS350 electrochemical workstation (Corrtest, China) with SCE as RE and a 40 × 60 mm stainless sheet as counter electrode (CE) installed in the left bath. A 10 mV sinusoidal signal over frequencies ranging from 100 kHz to 10 mHz was applied to the wire electrode around the OCP after it was disconnected from the WBE.

3. Results

3.1. Corrosion behaviour of WBE in 3% NaCl solution

3.1.1. Potential and galvanic mapping

Fig. 5 shows the potential and current maps of the WBE with time after $Ca(OH)_2$ solution in the left bath of the container (Fig. 3) was replaced by 3% NaCl solution. In the beginning (0 day), the mortar was free of Cl^- ions, the uppermost map in Fig. 5a shows that all wire electrodes are completely passivated, the potential distributions (−213.6 mV to −205.5 mV) are almost homogeneous, except that potential values at the WBE margins are slightly more positive due to higher oxygen content in the periphery of specimen.

Generally, the presence of chloride ions will shift the OCP of mild steel negatively [6]. After the solution in the left bath was replaced by 3% NaCl, several negative potential peaks appear in 3 days, along with a negative shift of the general OCP of the WBE from −210 mV to −250 mV, as shown in Fig. 5a. Meanwhile, anodic current was found on the wire electrodes with more negative potential. Since the OCP values of each wire electrode is more positive than −250 mV, the whole WBE should be passivated, which is confirmed by the weak galvanic current fluctuation in the upper plot of Fig. 5c. During the first 15 days, it is seen that the amplitude and frequency of the anodic current peaks increase with time and decease with distance from the NaCl containing bath (Fig. 3). Particularly, the left side in Fig. 5c has statistically more frequent and stronger anodic current peaks than the right side due to the left bath contains higher Cl^- ions concentration than the right one. These strong current peaks suggest that pitting corrosion possibly initiates on the WBE. Nevertheless, there is still an exception that a stronger anodic current emerges on the wire electrode at column 15 row 4 on day 3, which might be attributed to that the surface defects or inclusions (MnS or carbide) other than chloride ingression induce pitting corrosion on this wire electrode.

However, after 17 days, the general OCP of the WBE shifts negatively to ~−513.0 mV, suggesting that the WBE could be deprived of passivity. With the negative shift of the general OCP, the potential differences among all wire electrodes deceases (from top to bottom of Fig. 5b). Meanwhile, the anodic current peaks in Fig. 5d also attenuate after 17 days. As a matter of fact, since the dissolved oxygen diffuses through micro pores much slower than gaseous oxygen [30], once the mortar specimen was immersed in NaCl solution, water would penetrate and suffuse the micro pores in the mortar, thus the diffusion rate of oxygen in the mortar could fail to match the consumption

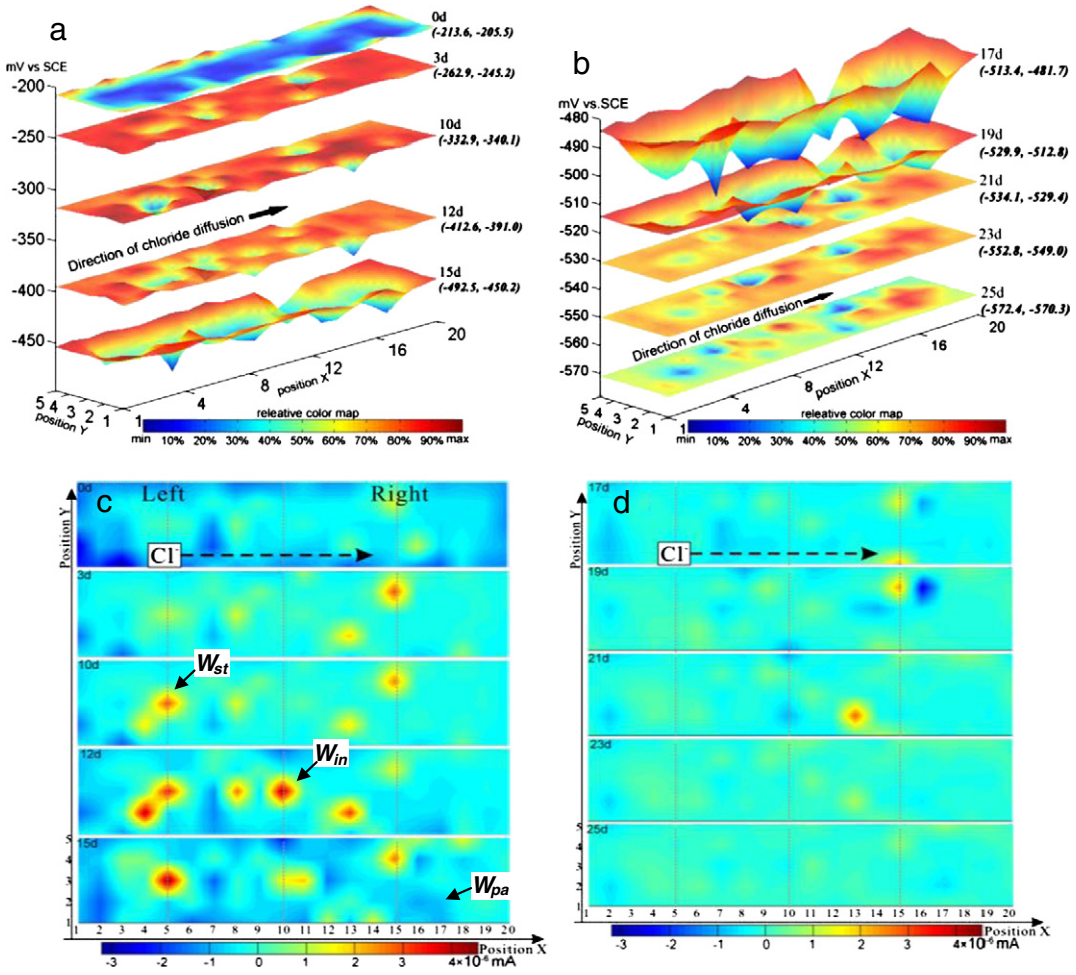

Fig. 5. Time dependence of the potential (a,b) and galvanic current (c,d) distributions on the WBE surface, the corresponding days of immersion (such as 15 d) and potential extreme values (such as −492.5 mV to −450.2 mV) are listed at the right side of every subplot.

(reduction) rate of oxygen, resulting in a severe depletion of oxygen in the mortar. Meanwhile, the anodic current of wire electrodes was mainly maintained by the cathodic reduction of residual oxygen in the mortar. After the dissolved oxygen in the mortar was exhausted, the anodic current attenuates quickly and the general OCP of the WBE moves negatively. Notice that the centre of the WBE has a stronger negative shift of OCP than the edges, indicating that the central region of the mortar specimen has lower oxygen content due to longer diffusion distance. After 25 days of immersion, the general OCP of the WBE moves negatively to −572 mV and the potential difference among wire electrodes decrease quickly (Fig. 4b), suggesting that the oxygen in the mortar could be completely depleted, which

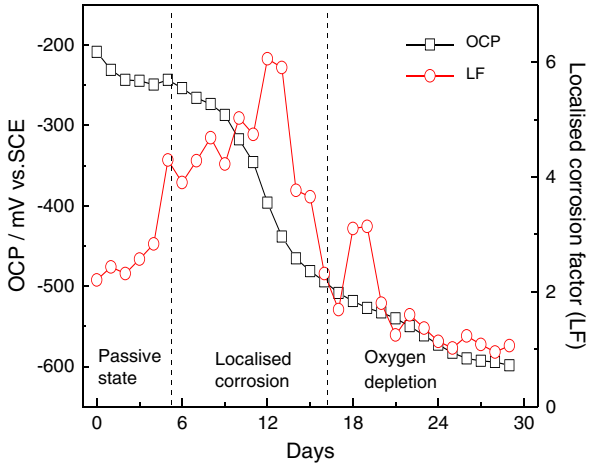

Fig. 6. *LF* value and general OCP of WBE as a function of time during the wetting drying process.

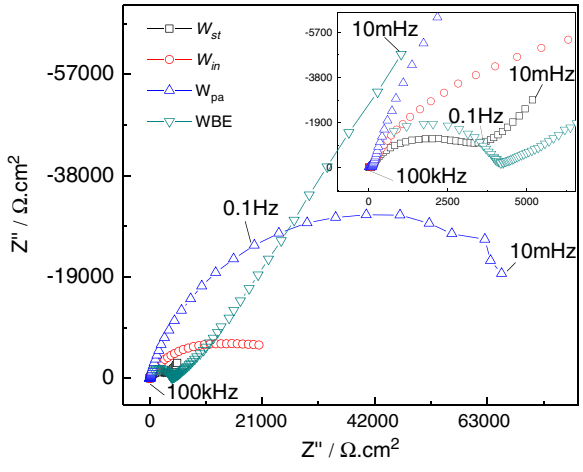

Fig. 7. EIS of three representative wire electrodes W_{st}, W_{in}, W_{pa} and EIS of the whole WBE in WBE-embedded mortar sample after 30 day wetting drying cycle.

not only smoothen both the potential and galvanic current maps, but also decrease the current amplitude dramatically.

In order to quantify the intensity of localized corrosion of rebar in mortar, *LF* values are calculated based on the current distribution in Fig. 5. The *LF* values and the general OCP of the WBE are plotted versus time in Fig. 6. It is seen that the *LF* value increases to its maximum (6.0) in 12 days, suggesting that the localized corrosion aggravates with time. However, after 12 days, the *LF* value gradually decreases to *ca.* 1, indicating that the heterogeneous corrosion mitigates. In the later stage of immersion, the depletion of oxygen in the mortar leads to a strongly negative shift of the general OCP and the attenuation of the anodic current, leading to the remission of the localised corrosion of WBE. Furthermore, Fig. 6 can be divided into three zones according to the general OCP value based on the ASTM-876C standard [31]. When the OCP is higher than −250 mV, no apparent corrosion occurs, when the OCP fluctuates between −250 mV and −500 mV, localized corrosion initiates. When the OCP is lower than −500 mV, it is believed that cathodic depolarization is

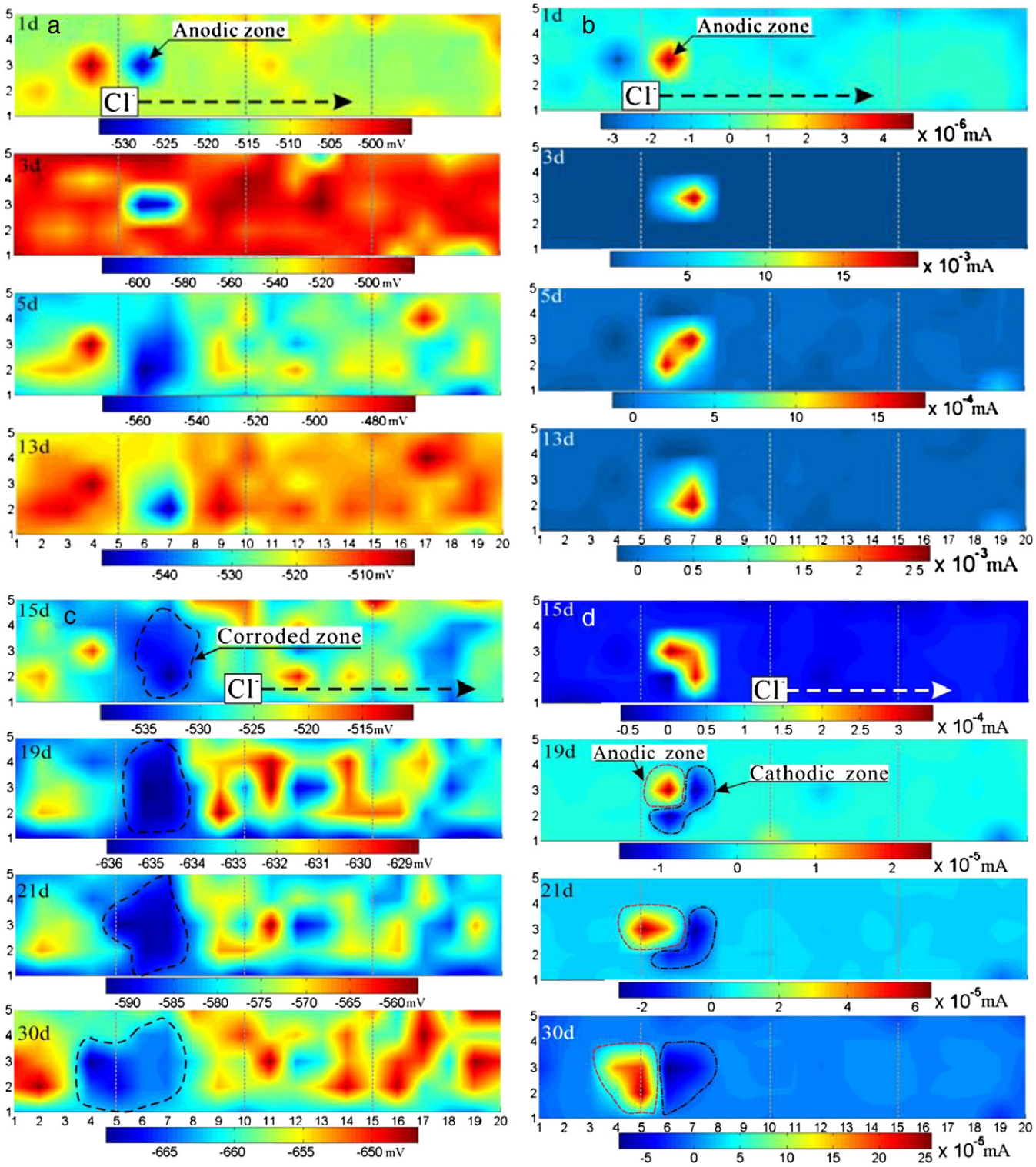

Fig. 8. Evolution of potential (a, c) and current (b, d) distributions of WBE in mortar during wetting–drying cycle.

remarkably inhibited due to oxygen depletion, resulting in the negative shift of OCP.

3.1.2. EIS of wire electrodes

Considering the emerging time and amplitude of anodic current in Fig. 5c, all electrodes in WBE can be classified as stably corroding electrode W_{st} (anodic current arising early), incipiently corroding electrode W_{in} (anodic current arising lately) and passive electrode W_{pa} (no anodic current throughout the test). For example in Fig. 5c, the wire electrode $W_{5,3}$ (representing the two-dimensional coordinate at column 5 row 3 in the WBE) can be regarded as W_{st} in view of that its anodic current emerged early on day 3. Similarly, the electrode $W_{10,3}$ can be regarded as W_{in} in view of its lately emerging anodic current.

In order to clarify the difference of corrosion behaviours of W_{st}, W_{in} and W_{pa} at the end of mapping test of 30 days, three wire electrodes representing W_{st}, W_{in} and W_{pa} were chosen for EIS measurement. EIS of each wire electrode was conducted just around its OCP other than the general OCP of WBE. Fig. 7 shows that W_{st} has the smallest impedance circle at high-frequency region and exhibits the characteristics of oxygen diffusion control due to the linear Warburg impedance at low-frequency region, indicating that W_{st} suffers serious corrosion, which is proven by the severely rusty wire electrode after the mortar cover was removed. On the other hand, the passive wire electrode W_{pa} has a large impedance circle, suggesting that the passive film on this electrode exhibits good corrosion resistance although its OCP below −600 mV. As expected, the corrosion resistance of the wire electrode W_{in} is just between W_{st} and W_{pa}. In addition, when all wire electrodes in WBE are interconnected together to form a one-piece working electrode, EIS of the WBE is also characteristic of typical Warburg diffusion impedance, further confirming that the WBE is under oxygen diffusion control.

3.2. Corrosion behaviour of WBE during wetting–drying cycle

3.2.1. Potential and galvanic mapping of WBE

Wetting–drying cycle has been widely applied to accelerate corrosion of rebar [32]. Generally, the diffusion of oxygen in water is much slower than in air. During wetting period, the oxygen content in the pore solution of mortar will decrease due to the cathodic reduction of oxygen, but during the drying period, the decreasing water content in the mortar would facilitate oxygen diffusion process [30]. Thus, the increasing oxygen could react with steel and rebuild the passive film of rebar in case that Cl^- content in mortar is lower than a threshold. If the Cl^- content exceeds the threshold, higher oxygen level may accelerate the localized corrosion of rebar during the following wetting period.

Fig. 8 shows the evolution of heterogeneous corrosion on the WBE embedded in mortar during wetting–drying cycle. In the first wetting period (24 h), an anodic zone (corresponding to more negative potential in Fig. 8a and more positive anodic current in Fig. 8b) emerges at the wire electrode $W_{6,3}$. On day 3, the anodic current zone shifts to $W_{7,3}$ from $W_{6,3}$. From day 3 to day 13, the anodic zone expands gradually, indicating a slow propagation of rust layer. However, after the 19th day, the successive current maps in Fig. 8d show that the earlier formed anodic zone (including wire electrodes $W_{6,2}$, $W_{6,3}$, $W_{7,2}$, $W_{7,3}$) gradually turn into cathodic zone, and a new anodic zone forms at the nearby electrodes $W_{4,3}$, $W_{5,3}$, $W_{5,2}$. Based on the current maps, this polarity conversion seemingly suggests that the corrosion on the early corroded zone is inhibited in view of its cathodic current. Nevertheless, the potential maps in Fig. 8c reveal that the "cathodic zone" exhibit more negative OCP than other zones, indicating that the anodic zone according to potential maps is inconsistent with that according to current maps. For instance, the wire electrode $W_{7,3}$ exhibits stronger cathodic current, but its potential is more negative than others. This conflict suggests that the early formed corrosion products (Fe_2O_3) covering the wire electrode $W_{6,2}$, $W_{6,3}$, $W_{7,2}$, $W_{7,3}$ could take part in the cathodic reduction as electron acceptor. Interestingly, from Fig. 8d, it is also seen that the strongest anodic zone is always adjacent to the strongest cathodic zone in the current maps, which is possibly attributed to that the high ohmic resistance of mortar limits the further transfer of current flow. Therefore, the anodic current is generally consumed by the cathodic reduction of O_2 on the wire electrodes nearby the corroded wire electrodes.

In order to verify the conversion of current polarity of the corroded zone, the WBE-embedded mortar sample was again immersed in 3% NaCl solution for 200 min and then dried naturally in air, the galvanic currents from the wire electrode W_{in} and W_{st} were successively monitored during this wetting–drying process, the time-dependent current curves are shown in Fig. 9. It can be seen that both current curves start at higher anodic currents in the beginning of immersion and then decrease gradually with the depletion of dissolved oxygen in the mortar. Interestingly, the galvanic current from the W_{st} even turns into cathodic after 100 min of immersion.

Galvanic current generally reflects the net result of anodic and cathodic reactions on a single wire electrode. In the presence of oxygen, the anodic dissolution of rebar could produce FeOOH (lepidocrocite) according to Eqs. (3) and (4). However, when the sample was immersed in NaCl solution, FeOOH could be reduced into Fe_3O_4 (magnetite) due to the lower oxygen level according to Eq. (6) [33]. Once the reduction current from the corrosion products covering W_{st} (Eq. (6)) exceeds the dissolution current of W_{st} (Eq. (3)), the measured current from W_{st} will become cathodic, as shown in Fig. 9.

$$\text{Oxidation}: \quad Fe \rightarrow Fe^{2+} + 2e^- \tag{3}$$

$$2Fe^{2+} + 1/2O_2(g) + H_2O(l) \rightarrow 2FeOOH(s) + 4e^- \tag{4}$$

$$\text{Reduction}: \quad O_2(g) + 2H_2O(l) + 4e^- \rightarrow 4OH^- \tag{5}$$

$$8FeOOH(s) + Fe^{2+} + 2e^- \rightarrow 3Fe_3O_4(s) + 4H_2O(l) \tag{6}$$

On the other hand, the net current from W_{in} is always anodic, which is possibly attributed to that the reduction current from iron oxides (FeOOH or Fe_2O_3) is less than the anodic current from the dissolution of W_{in} due to no enough reducible corrosion products on the surface of W_{in}.

After the WBE has been taken out and dried in air for 60 min, the wire electrode W_{st} recovers its anodic polarity, suggesting that the reduction of replenished oxygen on other wire electrodes predominates

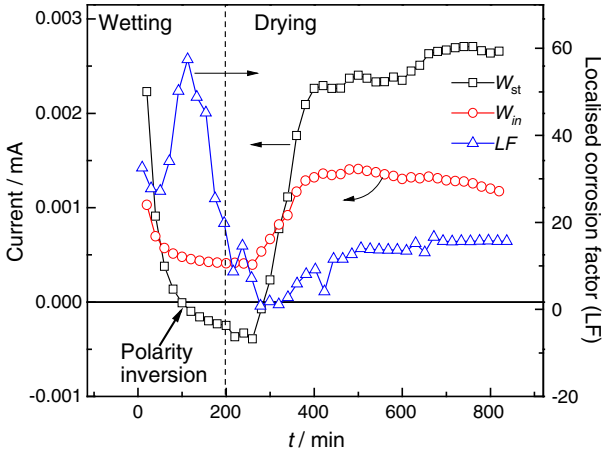

Fig. 9. Time dependence of galvanic current from the wire electrodes W_{in} and W_{st} during wetting–drying cycle.

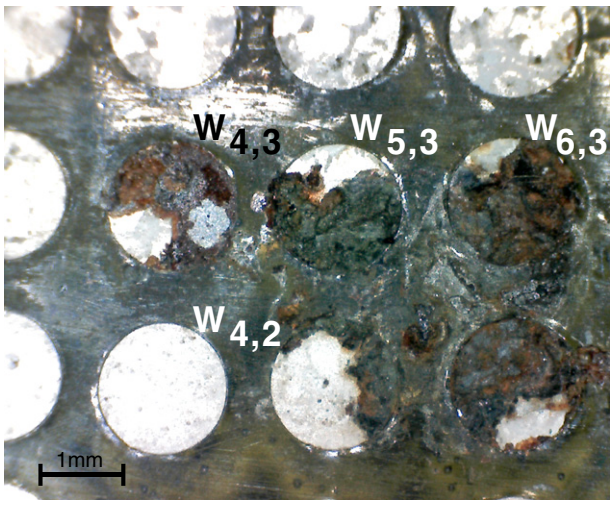

Fig. 10. Morphology of corrosion products on the WBE after mortar cover removed, the symbol such as $W_{4,3}$ represent the coordinate of line and column of a wire electrodes on the WBE.

again over that of the corrosion products on W_{st} in the WBE. Meanwhile, Fe^{2+} ions of corrosion products will be oxidised into Fe^{3+} ions according to Eq. (4), i.e. the corrosion products on W_{st} will restore their oxidability and act as cathodic depolariser during next wetting period.

Fig. 9 also shows that both anodic currents from W_{in} and W_{st} increase with time during the following drying period, indicating that the increasing oxygen level promotes the dissolution of the corroded electrodes. The higher anodic current from W_{st} than that from W_{in} is also consistent with the lower impedance of W_{st} in Fig. 7. In addition, along with the current polarity inversion of W_{st}, the *LF* value increases quickly to the highest in the wetting period, which is possibly due to that the anodic current becomes more concentrated on the W_{in}, as shown in Fig. 8b. However, during the drying period, the *LF* value decreases with time and stabilizes eventually, suggesting that the current distribution on the WBE becomes uniform due to that the increase in the overall anodic currents of WBE reduces the fluctuation range of current. Thus, the *LF* index may reflect the heterogeneity of apparent anodic current.

3.3. Analysis of corrosion products

Fig. 10 shows the distribution of corrosion products on wire electrodes after mortar layer on the WBE was removed. Fe^{2+} ions from a corroding wire electrode (such as $W_{6,3}$) diffuse out through pores in the mortar, then react with OH^- ions and O_2 in pore solution, forming insoluble corrosion products [16]. Corrosion products accumulate mainly in the micro pores along the steel/mortar interface, the resulting volumetric expansion gives rise to the propagation of cracks and a further inclusion of aggressive species [34], which would exacerbate the corrosion of rebar. According to our previous work [35], when corrosion products spread to a vicinal uncorroded (passive) wire electrode (such as $W_{5,3}$, $W_{4,3}$ in Fig. 8), it would initiate pitting corrosion of the passive wire electrode due to the high Cl^- ion level around it, since the corrosion products have a strong Cl^- ions adsorption and cathodic depolarization ability.

Raman spectroscopy has been widely applied to analyse corrosion products [19,36]. Fig. 11a and b shows the laser focus areas for micro-Raman spectra analysis on the wire electrodes W_{in} (i.e. $W_{5,3}$)

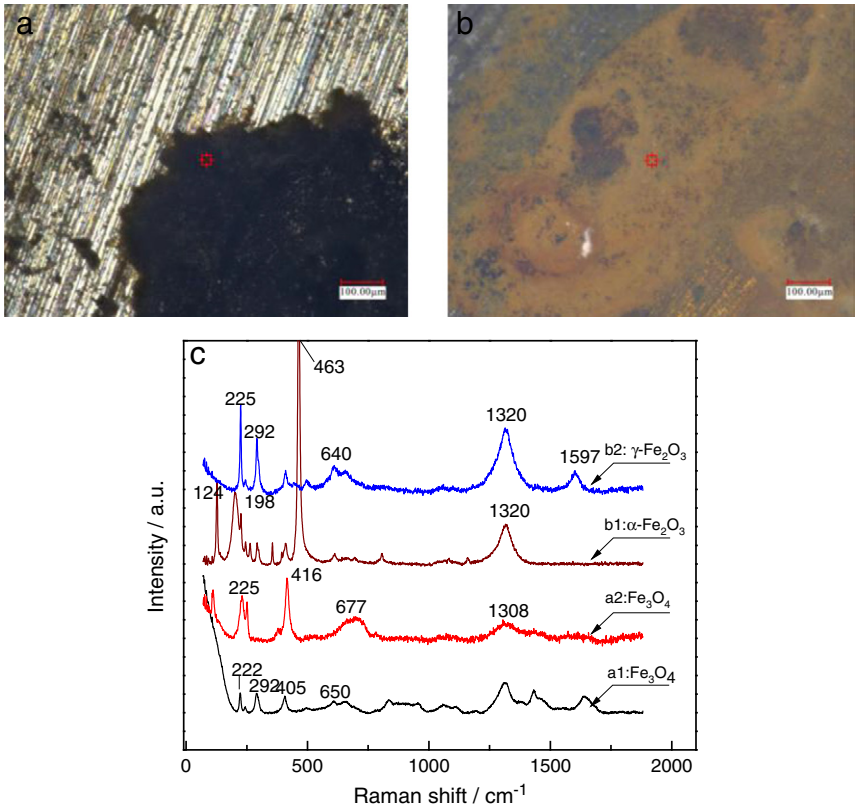

Fig. 11. Micrographs of an incipiently corroding wire electrode W_{in} (a) and a stably corroded wire electrode W_{st} (b) on the WBE. The arrowed mark indicates the focus (ca. 1 mm diameter) of micro Raman analysis. The Raman spectra of corrosion products on the corresponding wire electrodes are showed with a1, a2 and b1, b2 representing the analytical sequence at W_{in} and W_{st}, respectively (c).

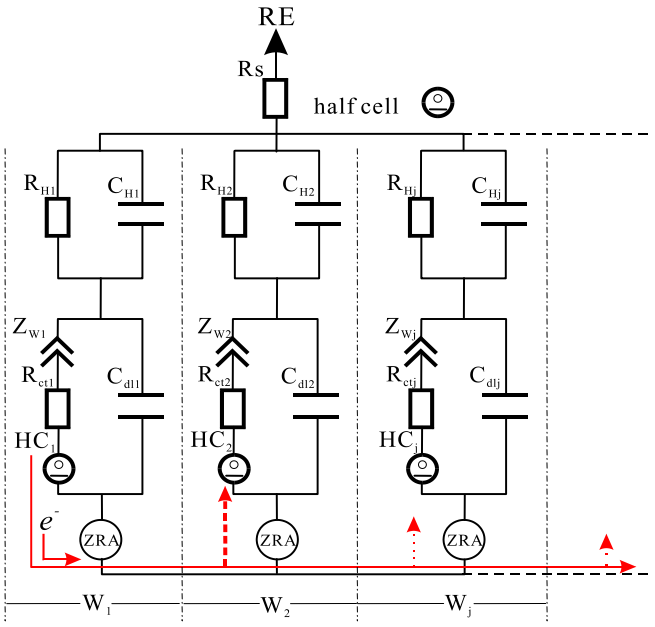

Fig. 12. Equivalent circuit of the WBE-embedded in mortar, each wire electrode (W_1,W_2,W_j) is represented by a subcircuit, where $Z_{w,j}$, $R_{ct,j}$,HC_j and C_{dlj} are the Warburg component, charge transfer resistance, half cell and double layer capacitance in the jth subcircuit, respectively. $R_{H,j}$, $C_{H,j}$ and R_s are the mortar resistance, mortar capacitance and solution resistance respectively.

and W_{st} (i.e. $W_{6,3}$). It is seen that the corrosion product on W_{in} looks like black but that on W_{st} looks like yellowish, suggesting that the latter could be further oxidised into hematite (Fe_2O_3). The micro-Raman spectra are shown in Fig. 11c, where the intense band at 1320 cm^{-1} is assigned to a two-magnon scattering arising from anti-ferromagnetic structure of hematite [36]. Characteristic peaks at 665–680 cm^{-1} are attributed to the magnetite, and low intensity bands (124, 225, 292, 405 and 463 cm^{-1}) are attributed to the hematite phase. It confirms that the main composition of rust layer is α-Fe_2O_3 on W_{st}, and Fe_3O_4 on W_{in}.

4. Discussions

The mismatch of potential and current maps in Fig. 8 was rarely reported because most researches about WBE technique focused only on the corrosion in electrolytic solution [29]. However, the corrosion behaviour underneath concrete cover is totally different due to the high diffusion resistance and heterogeneity of cement phase.

Fig. 12 shows an equivalent circuit for the coupled WBE, where each wire electrode is represented by a subcircuit and all subcircuits are interconnected parallelly through ZRAs. A half-cell HC_j is introduced to represent the electrochemical half reaction on jth wire electrode. The driving force of the current flows in/out a wire electrode depends on the potential difference between half-cells and the impedance of each subcircuit. During the anodic dissolution of W_j, electrons will flow out of W_j to other wire electrodes having a lower loop ohmic resistance ($R_{H,j}$) to W_j. Generally, the ohmic resistance through mortar determines how far the current flow travels. Therefore, wire electrodes very close to W_j often consume much more electrons from W_j via oxygen cathodic reduction, as shown in the current maps of Fig. 8d. However, during the wetting period, oxygen depletion not only makes the general OCP of WBE shift negatively but also inhibits the cathodic reaction of corrosion. Then FeOOH or Fe_2O_3 in corrosion products instead of oxygen will take part in the cathodic reaction as reducer. If the cathodic current from the reduction of Fe (III) oxides exceeds the anodic current from the dissolution of a wire electrode, the wire electrode would exhibit net cathodic current, as shown in Fig. 8d.

Fig. 13a proposes a model for the corrosion propagation on WBE. During the drying period, micro pores in mortars will lose partially water and be refilled with air. Increasing oxygen content then accelerates the corrosion of both W_{st} and W_{in} and the oxidization of Fe (II) oxides of corrosion products. By using the isotopic tracer method (^{18}O), Burger et al. also demonstrated that ^{18}O were mainly enriched at the metal/corrosion product interface, indicating the oxidation of magnetite at the inlayer of corrosion product [13]. During the wetting period (Fig. 13b), the micro pores are saturated by water, resulting in the depletion of oxygen at the interface of mortar/steel. Thus, Fe (III) oxides (FeOOH) covering the wire electrodes W_{st} replace oxygen as a cathodic depolariser to maintain the corrosion. Furthermore, an occluded zone may form between the accumulated corrosion product layer and the steel base during wetting–drying cycle [37]. Hence, the so-called "auto-acidulation effect" will accelerate corrosion of the wire electrodes W_{in}.

Fe^{2+} ions can spread out along the micro pores of mortar, and then react with dissolved oxygen or OH^- ions to form corrosion precipitate. Considering that the corrosion products have strong Cl^- ion absorbability [35], once the concentration ratio of enriched Cl^- to OH^- ions exceeds a threshold around the corrosion products, it possibly initiates new pitting corrosion on the passive wire electrodes in touch with the corrosion products [35]. Thus, new corrosion site grows and merges with the old corrosion sites, resulting in horizontal expansion of corrosion area along the interface of mortar and rebar, as shown in Fig. 10.

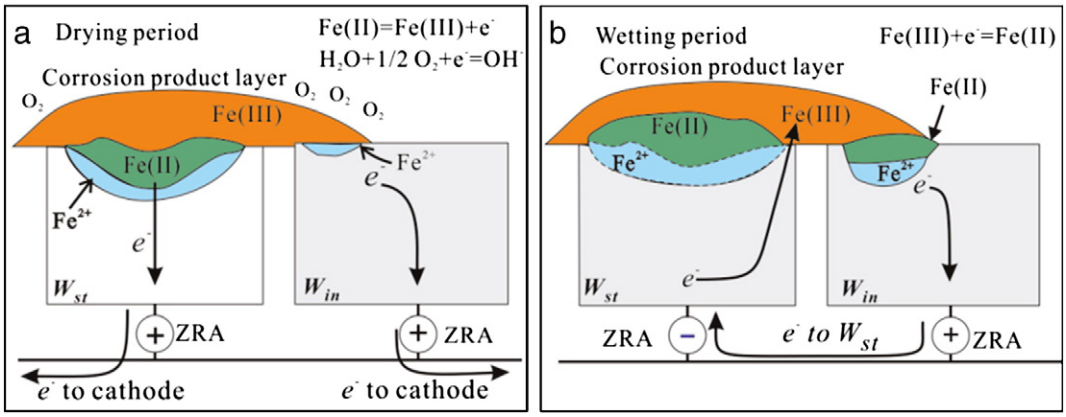

Fig. 13. The schematic diagram of spreading corrosion products in a wetting–drying cycle, the arrow representing direction of electron transfer during the redox of Fe(III)/Fe(II), the symbols of "+" and "−" representing the anodic and the cathodic current, respectively.

5. Conclusion

A wire beam electrode (WBE) technique was applied to study the localized corrosion of rebar under mortar cover. The immersion test showed that the general OCP of wire electrodes embedded in mortar shifted negatively with time due to the oxygen depletion. Meanwhile, potential and galvanic current distributions of the WBE also tended to be flat due to the attenuation of the cathodic depolarization in wet mortar. In addition, a lower *LF* value deduces that the heterogeneity of rebar corrosion in underwater concrete may be mitigated due to the limited oxygen content.

Wetting–drying cycle can promote the corrosion of WBE in mortar. FeO or Fe_3O_4 in corrosion products can be oxidised to FeOOH by oxygen in the drying period and then be reduced into Fe (II) oxides in the wetting period, i.e. the corrosion products can replace partially dissolved oxygen to maintain rebar corrosion in oxygen-deficient wet mortar.

Corrosion products can initiate new pitting corrosion on the surface of passive wire electrodes, but the high ohmic resistance of mortar limits the galvanic current travelling to farther wire electrodes, leading to that the strongest anodic zone often emerges nearby the strongest cathodic zone along the interface of rebar and mortar.

Acknowledgements

This research was supported by the National Natural Science Foundation of China (Project No. 50478011).

References

[1] P. Dangla, W. Dridi, Rebar corrosion in carbonated concrete exposed to variable humidity conditions. Interpretation of Tuutti's curve, Corros. Sci. 51 (2009) 1747–1756.
[2] H.E. Jamil, M.F. Montemor, R. Boulif, A. Shriri, M.G.S. Ferreira, An electrochemical and analytical approach to the inhibition mechanism of an amino-alcohol-based corrosion inhibitor for reinforced concrete, Electrochim. Acta 48 (2003) 3509–3518.
[3] U. Angst, B. Elsener, C.K. Larsen, O. Vennesland, Critical chloride content in reinforced concrete — a review, Cem. Concr. Res. 39 (2009) 1122–1138.
[4] H. Yu, X.M. Shi, W.H. Hartt, B.T. Lu, Laboratory investigation of reinforcement corrosion initiation and chloride threshold content for self-compacting concrete, Cem. Concr. Res. 40 (2010) 1507–1516.
[5] M.B. Valcarce, M. Vazquez, Carbon steel passivity examined in solutions with a low degree of carbonation: the effect of chloride and nitrite ions, Mater. Chem. Phys. 115 (2009) 313–321.
[6] P. Ghods, O.B. Isgor, G.A. Mcrae, G.P. Cu, Electrochemical investigation of chloride-induced depassivation of black steel rebar under simulated service conditions, Corros. Sci. 52 (2010) 1649–1659.
[7] M. Ormellese, M. Berra, F. Bolzoni, T. Pastore, Corrosion inhibitors for chlorides induced corrosion in reinforced concrete structures, Cem. Concr. Res. 36 (2006) 536–547.
[8] U.M. Angst, B. Elsener, C.K. Larsen, O. Vennesland, Chloride induced reinforcement corrosion: electrochemical monitoring of initiation stage and chloride threshold values, Corros. Sci. 53 (2011) 1451–1464.
[9] M. Sanchez, J. Gregori, C. Alonso, J.J. Garcia-Jareno, H. Takenouti, F. Vicente, Electrochemical impedance spectroscopy for studying passive layers on steel rebars immersed in alkaline solutions simulating concrete pores, Electrochim. Acta 52 (2007) 7634–7641.
[10] W. Wang, Y.H. Lu, Y. Zou, X. Zhang, J. Wang, The heterogeneous electrochemical characteristics of mild steel in the presence of local glucose oxidase—a study by the wire beam electrode method, Corros. Sci. 52 (2010) 810–816.
[11] Y.J. Tan, An experimental comparison of three wire beam electrode based methods for determining corrosion rates and patterns, Corros. Sci. 47 (2005) 1653–1665.
[12] J.A. González, J.M. Miranda, E. Otero, S. Feliu, Effect of electrochemically reactive rust layers on the corrosion of steel in a Ca(OH)(2) solution, Corros. Sci. 49 (2007) 436–448.
[13] E. Burger, J. Monnier, P. Berger, D. Neff, V. L'Hostis, S. Perrin, P. Dillmann, The long-term corrosion of mild steel in depassivated concrete: localizing the oxygen reduction sites in corrosion products by isotopic tracer method, J. Mater. Res. 26 (2011) 3107–3115.
[14] K. Videm, Phenomena disturbing electrochemical corrosion rate measurements for steel in alkaline environments, Electrochim. Acta 46 (2001) 3895–3903.
[15] J. Wang, Y. Zou, Y.Y. Zheng, Electrochemical techniques for determining corrosion rate of rusted steel in seawater, Corros. Sci. 53 (2011) 208–216.
[16] H.S. Wong, Y.X. Zhao, A.R. Karimi, N.R. Buenfeld, W.L. Jin, On the penetration of corrosion products from reinforcing steel into concrete due to chloride-induced corrosion, Corros. Sci. 52 (2010) 2469–2480.
[17] D. Koleva, J. Hu, A. Fraaij, P. Stroeven, N. Boshkov, J. De Wit, Quantitative characterisation of steel/cement paste interface microstructure and corrosion phenomena in mortars suffering from chloride attack, Corros. Sci. 48 (2006) 4001–4019.
[18] Z.H. Dong, W. Shi, G.A. Zhang, X.P. Guo, The role of inhibitors on the repassivation of pitting corrosion of carbon steel in synthetic carbonated concrete pore solution, Electrochim. Acta 56 (2011) 5890–5897.
[19] X.H. Nie, X.G. Li, C.W. Du, Y.Z. Huang, H. Du, Characterization of corrosion products formed on the surface of carbon steel by Raman spectroscopy, J. Raman Spectrosc. 40 (2009) 76–79.
[20] Y. El Mendili, J.F. Bardeau, N. Randrianantoandro, A. Gourbil, J.M. Greneche, A.M. Mercier, F. Grasset, New evidences of in situ laser irradiation effects on γ-Fe2O3 nanoparticles: a Raman spectroscopic study, J. Raman Spectrosc. 42 (2011) 239–242.
[21] A. Poursaee, Corrosion of steel bars in saturated Ca(OH)2 and concrete pore solution, Concr. Res. Lett. 1 (2010) 90–97.
[22] Y.J. Tan, N.N. Aung, T. Liu, Novel corrosion experiments using the wire beam electrode. (I) Studying electrochemical noise signatures from localised corrosion processes, Corros. Sci. 48 (2006) 23–38.
[23] N.N. Aung, Y.J. Tan, T. Liu, Novel corrosion experiments using the wire beam electrode: (II) Monitoring the effects of ions transportation on electrochemical corrosion processes, Corros. Sci. 48 (2006) 39–52.
[24] L.B. Mechmeche, L. Dhouibi, M. Ben Ouezdou, E. Triki, F. Zucchi, Investigation of the early effectiveness of an amino-alcohol based corrosion inhibitor using simulated pore solutions and mortar specimens, Cem. Concr. Compos. 30 (2008) 167–173.
[25] A. Nasser, A. Clement, S. Laurens, A. Castel, Influence of steel-concrete interface condition on galvanic corrosion currents in carbonated concrete, Corros. Sci. 52 (2010) 2878–2890.
[26] N.N. Aung, Y.J. Tan, Monitoring pitting-crevice corrosion using the WBE-noise signatures method, Mater. Corros. 57 (2006) 555–561.
[27] E.C. Almeida, A.V. Diniz, V.J. Trava-Airoldi, N.G. Ferreira, Electrochemical characterization of doped diamond-coated carbon fibers at different boron concentrations, Thin Solid Films 485 (2005) 241–246.
[28] Z.H. Dong, W. Shi, H.M. Ruan, G.A. Zhang, Heterogeneous corrosion of mild steel under SRB-biofilm characterised by electrochemical mapping technique, Corros. Sci. 53 (2011) 2978–2987.
[29] N.N. Aung, Y.J. Tan, A new method of studying buried steel corrosion and its inhibition using the wire beam electrode, Corros. Sci. 46 (2004) 3057–3067.
[30] B. Huet, V. L'hostis, G. Santarini, D. Feron, H. Idrissi, Steel corrosion in concrete: determinist modeling of cathodic reaction as saturation a function of water degree, Corros. Sci. 49 (2007) 1918–1932.
[31] ASTM, Standard Test Method for Corrosion Potentials of Uncoated Reinforcing Steel in Concrete, C876-09, 2009, pp. 446–451.
[32] R. El-Hacha, A. Mirman, A. Cook, S. Rizkalla, Effectiveness of surface-applied corrosion inhibitors for concrete bridges, J. Mater. Civ. Eng. 23 (2011) 271.
[33] R. Vera, M. Villarroel, A.M. Carvajal, E. Vera, C. Ortiz, Corrosion products of reinforcement in concrete in marine and industrial environments, Mater. Chem. Phys. 114 (2009) 467–474.
[34] S.J. Jaffer, C.M. Hansson, Chloride-induced corrosion products of steel in cracked-concrete subjected to different loading conditions, Cem. Concr. Res. 39 (2009) 116–125.
[35] Z.H. Dong, W. Shi, X.P. Guo, Initiation and repassivation of pitting corrosion of carbon steel in carbonated concrete pore solution, Corros. Sci. 53 (2011) 1322–1330.
[36] D.L.A. de Faria, S. Venâncio Silva, M.T. de Oliveira, Raman microspectroscopy of some iron oxides and oxyhydroxides, J. Raman Spectrosc. 28 (1997) 873–878.
[37] T. Pastore, M. Cabrini, L. Coppola, S. Lorenzi, P. Marcassoli, A. Buoso, Evaluation of the corrosion inhibition of salts of organic acids in alkaline solutions and chloride contaminated concrete, Mater. Corros. 62 (2011) 187–195.